Extremely high fatigue resistance in an ultrafine grained high entropy alloy

K. Liu[a], S.S. Nene[a], M. Frank[a], S. Sinha[a], R.S. Mishra[a,b,*]

[a]Center for Friction Stir Processing, Department of Materials Science and Engineering
University of North Texas, Denton, Texas 76203 USA

[b]Advanced Materials and Manufacturing Processes Institute
University of North Texas, Denton, Texas 76203 USA

*Corresponding author: Rajiv.Mishra@unt.edu

Abstract

Fatigue of structural materials is a leading cause of failure and has motivated fatigue-resistant design to eliminate risks to human lives. Majority of conventional materials, including advanced steels and Ni-based superalloys, exhibit limited fatigue endurance limits at ambient temperature. With this in mind, we designed a Cu-containing FeMnCoCrSi high entropy alloy which exhibits a normalized fatigue ratio of ~ 0.62 UTS (ultimate tensile strength). Our design approach was based on (a) engineering the γ phase stability to attain sustained work hardening (WH) through delayed γ (f.c.c.) →ε (h.c.p.) transformation to hinder fatigue crack propagation and (b) an ultrafine grained (UFG) microstructure to delay crack initiation. We verified that a UFG γ dominant microstructure could provide opportunities for enhanced fatigue resistance, as sustained WH activity strengthened the material locally in the crack plastic zone, thereby validating our expectation that the combination of UFG and transformation induced plasticity (TRIP) is a path to design the next generation of fatigue-resistant alloys.

Keywords: Fatigue resistant; deformation mechanisms; ultrafine grained; TRIP

Introduction

Fatigue is known as a damage accumulation process that results in catastrophic failure of structural materials, and that eventually threatens human safety. Therefore, designing fatigue-resistant materials to counteract or at least to mitigate compromises to human safety is imperative. Classically, total fatigue life has been improved by controlling microstructure to increase fatigue crack initiation life and to reduce the crack propagation rate [1]. Refinement of the grain size results in a higher resistance to crack initiation, thereby improving fatigue initiation life. Through this approach, high cycle fatigue property is enhanced. However, ultrafine grained materials are known to exhibit higher crack growth rate, which results in lower fatigue propagation life, and ultimately results in poor response at higher stress amplitude [2]. To overcome this significant deficiency, additional mechanisms can be used to arrest or retard crack propagation by localized work hardening (WH) activity within the crack tip plastic zone [3-5]. Koyama et al. [6] reported that a bone-like laminated microstructure in a metastable steel could assist in arresting fatigue crack growth by activating roughness-induced crack termination and transformation-induced crack termination micro-mechanisms and ultimately improving the alloy's fatigue property. Similarly, Ni-based superalloys show excellent fatigue property at high temperature owing to reduced grain size and delayed crack growth rate by coarsened γ'', β, γ'precipitates [7].

Recently, materials scientists have diverted away from the conventional alloy design strategy leading to a new class of materials, which are termed as high entropy alloys (HEAs), or complex concentrated alloys (CCAs) [8]. The conventional alloy design approach was to achieve a specific material property by interchanging the alloying element in the principle alloying element. Adding different elements alters materials' stacking fault energy, and eventually makes

it susceptible to sensitive phase stability with strain and temperature that alters the WH behavior of an alloy [8,9].

Microstructural features such as dislocations, twins, stacking faults, dispersoids and precipitates can provide paths for crack nucleation and propagation via their mutual interaction with the matrix under cyclic loading leading to fatigue failure. However, HEA design strategy provides abundant compositional space for either suppressing or eliminating these detrimental microstructural features for better fatigue properties. Stacking fault energy can be varied substantially by varying the mixing entropy (i.e. by changing the alloy chemistry) of the FCC matrix which allows activation of various deformation micro-mechanisms within the crack tip plastic zone, for example, twinning [10] and/or transformation [11]. When triggered, these mechanisms dissipate the energy available for crack growth, resulting in slower crack growth rate. Also, they locally strengthened the material through creation of additional interfaces. Few reports till date have studied and proved excellent fatigue properties of HEAs/CCAs, due to the formation of nanotwins near the crack [10,12,13], as well as by enhancing crack path tortuosity through hierarchically structured secondary phases [14]. Interestingly, combining twinning induced plasticity (TWIP) / transformation induced plasticity (TRIP) with conventional slip in HEAs led to enhanced WH behavior where uniform elongation was augmented with the assistance of strain-induced γ (f.c.c.) $\rightarrow\varepsilon$ (h.c.p.) transformation. The formation of α' martensite and ε-martensite are interdependent phenomena. However, their stability is dictated by the presence of certain alloying elements. For example, presence of Mn and Ni in austenite matrix. As observed in TRIP stainless steels with high fraction of Ni than Mn, α' martensite forms frequently whereas Ni –free TRIP steels with low, medium and high Mn content always showed

preferential ε formation [15,16]. Our recent works on design of microstructurally flexible HEAs based on metastability engineering by addition of Si in FeMnCoCr matrix showed adaptive phase stability of thermodynamically unstable ε phase (or stable γ phase), depending on alloy chemistry and processing conditions [17-19]. Thermodynamic simulations using ThermoCalc with the TCHEA2 database suggest that Si addition significantly alters the predicted γ phase stability and subsequent experimental results validated this by showing improved mechanical properties via extensive TRIP effect [18]. Due to strain induced transformation, we proved that the crack tip plastic zone altered WH locally, and improved the material's ability to compensate accumulated energy from fatigue damage [11].

Here we propose a combined alloy design and microstructural engineering strategy aimed at attaining superior fatigue performance. The present strategy promotes the desired response by resistance to the fatigue crack: (1) initiation by reducing grain size to oppose activation of lattice dislocations, and (2) propagation resistance by additional energy absorption due to strain-induced transformation in the plastic zone ahead of the crack tip. This aim was realized by the design of FeMnCoCrSi HEA having minor addition of Cu. This aim was realized by the design of FeMnCoCrSi HEA having minor addition of Cu. Minor addition of Cu makes the γ matrix more stable if dissolved in solid solution or can destabilize it if it forms clusters at the grain boundaries due to lack of solubility [20]. Thus, we used FSP as a microstructural engineering route since severe shear driven transport of elements during FSP can dissolve immiscible Cu in FeMnCoCrSi matrix thereby stabilizing the γ matrix.

Materials and Methods

The $Fe_{38.5}Mn_{20}Co_{20}Cr_{15}Si_5Cu_{1.5}$ (henceforth designated as Cu HEA) was produced by a vacuum induction melting in a cold-copper crucible backfilled with argon to 1 atm. The nominal composition of Cu-HEA is $Fe_{38.5}Mn_{20}Co_{20}Cr_{15}Si_5Cu_{1.5}$ (at. %), with a final dimension of the cast material 250 mm × 80 mm × 10 mm. The cast material was friction stir processed with a W-Re tool using the parameters listed in Table 1. The processing tool had a shoulder diameter of 12 mm with a tapered pin. The root diameter, pin diameter, and length of the tool were 7.5 mm, 6 mm, and 3.5 mm, respectively.

Table 1. Processing parameters selected for friction stir processing

Processing parameters	**Pass 1**	**Pass 2**
Tool Rotational Rate (RPM)	100	100
Traverse Speed (mm/min)	50.8	50.8
Plunge Depth (mm)	3.85	3.85
Tilt Angle (°)	2.0	2.0

Detailed microstructural analysis was carried out with back-scattered electron microscopy (BSE) using FEI Nova NanoSEM230. EBSD scans were done using orientation imaging microscopy (OIM) on FEI Nova NanoSEM230 to reveal the grain size and distribution and phase with 20 kV accelerating voltage and 6.1 nA current with step size 75 nm. Phases in the microstructure as presented were further confirmed with X-ray diffraction (XRD) measurements using RIGAKU X-Ray equipment, with Cu K_α radiation operated at 40 kV and 30 mA. To ensure homogeneity in the gage, mini tensile and fatigue samples were obtained from the nugget region 1 mm below the processed top surface. Mini tensile and fatigue samples were machined

using a computer numerical control machine. The tensile samples with gage length ~5 mm, width ~1.2 mm, and thickness ~1.1 mm were tested at room temperature using a computer-controlled mini-tensile machine at an initial strain rate of 10^{-3} s^{-1}. Fully reversed (R = -1) bending fatigue tests were performed with a custom-made tabletop fatigue testing machine at 20 Hz. Sample dimensions and machine details are given in [4]. Tensile and fatigue samples were polished with SiC papers to 1200 grit, and final polishing with 1 µm diamond suspension. Fatigue and microscopy samples were further polished with 0.05 and 0.02 µm colloidal silica suspensions.

Results and discussion

Besides grain refinement, friction stir processing (FSP) is a unique high-temperature severe deformation process wherein shear-driven transport of elements can dissolve immiscible elements into solid solution [21], and hence the expectation is that FSP could dissolve the immiscible Cu in the Fe-Mn-Co-Cr-Si matrix. Dissolution of Cu stabilizes the γ phase. The effect of Cu addition on grain and phase evolution in as-cast as well as as-FSP condition has been captured in Fig.1. Fig.1a_1 shows an electron backscatter diffraction (EBSD) inverse pole figure (IPF) map of the as-cast condition, where coarse grains with lath features were observed. Fig.1a_3 confirms the existence of ~15% ε phase. Knowing that FSP is a path to achieve ultrafine grain in alloys [5,22], two overlapping runs with tool rotational rate of 100 RPM were used. This resulted not only in extreme grain refinement (0.77 ± 0.35 µm) (Fig.1b) but also in a γ phase dominant microstructure (Figs.1c_1, c_3). Further, as expected, atom probe tomography confirmed homogeneous distribution of Cu in solid solution upon FSP without clustering or solute partitioning (Fig.1d). Dissolution of Cu in solid solution made the γ matrix more stable and

strong; a substantial contribution by solid solution strengthening. γ matrix stability was further confirmed by XRD showing stronger and more distinct peaks for the γ phase than the ε phase in both as-cast and as-FSP conditions (Figs.1a_2, c_2).

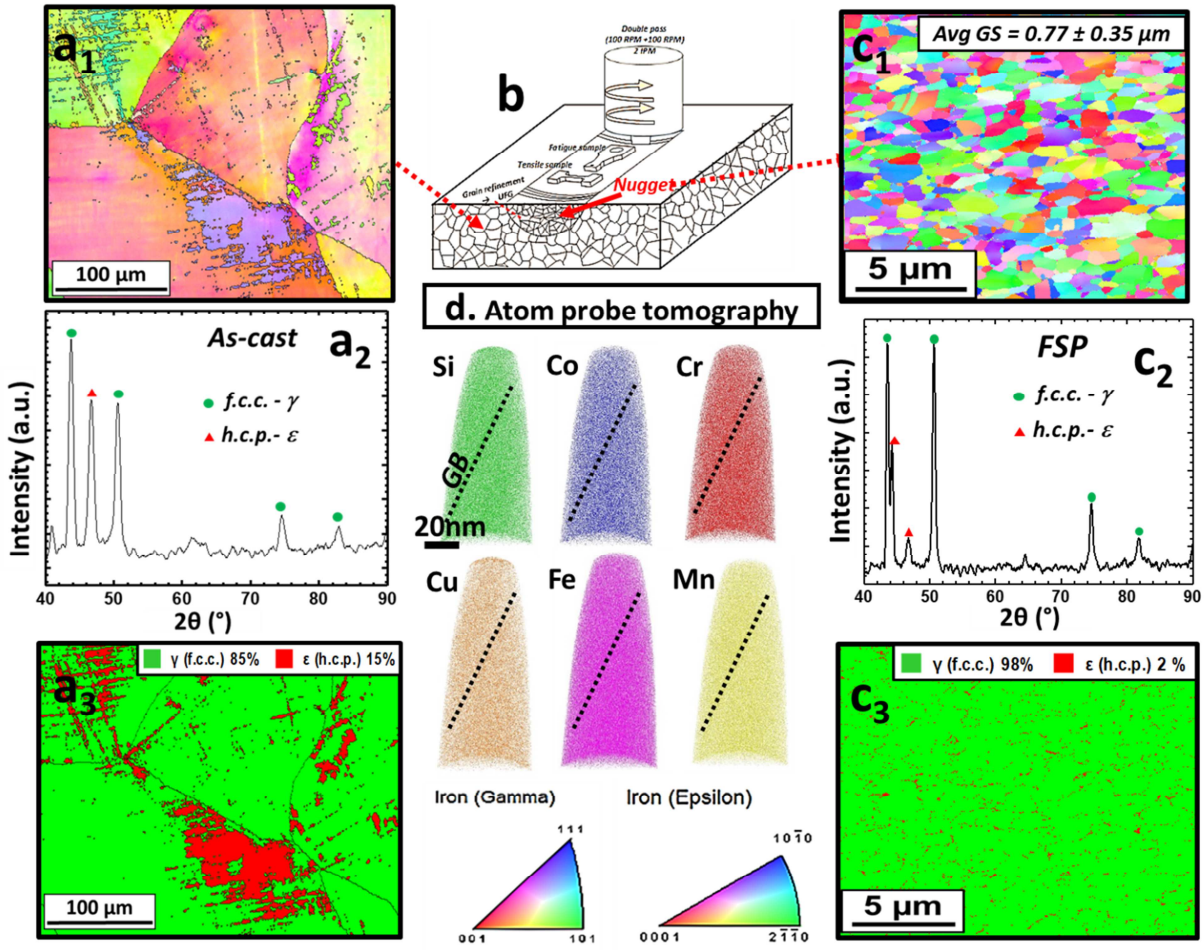

Fig.1. Microstructural evolution in Cu-HEA. (a_1) IPF map in the as-cast condition, (a_2) XRD pattern of the as-cast condition, (a_3) EBSD phase map in the as-cast condition, (b) schematic of friction stir processing and specimen orientation for tensile and fatigue testing, (c_1) IPF map in the nugget region, (c_2) XRD pattern of the FSP material, (c_3) EBSD phase map in the FSP material, (d) APT analysis showing elemental distribution at grain interior and boundary from the nugget region. (IPF: inverse pole Figure, XRD: X-ray diffraction, FSP: friction stir processing, EBSD: electron backscattered diffraction, APT: atom probe tomography)

The fatigue property of an alloy is closely related to its tensile response; hence, Fig.2a shows the engineering and true stress-strain curve for Cu-HEA in the as-FSP condition. The designed alloy has shown yield strength (YS) of ~850 MPa, ultimate tensile strength (UTS) of ~1126 MPa, and total elongation of ~42% (Fig.2a). Enhanced YS is an outcome of severe grain refinement, whereas increased UTS and ductility are attributed to a higher work hardenability [18,23] . The difference in the area under the red and blue curves hints to the work hardenability of Cu-HEA. The larger grain boundary area is expected to exert higher back stress for the ε plate to grow against the grain boundaries and hence causes local strain mismatch during deformation induced $\gamma \rightarrow \varepsilon$ transformation. As a result, this local grain boundary/ε plate interface activity triggers sustained yet slower WH via TRIP, and gives rise to UTS of ~1126 MPa and total elongation of ~42%. Further, excellent work hardenability could also alter the cyclic loading response of the Cu-HEA in spite of having ultrafine grain (UFG) size by manipulating the crack initiation and propagation behavior locally.

Typical UFG materials, with relatively increased numbers of grain boundaries, exhibit poor fatigue life in the low cycle fatigue (LCF) regime owing to rapid energy dissipation through favored crack propagation along these grain boundaries. Conversely, in the high cycle fatigue (HCF) regime, the fatigue endurance limit of UFG materials is enhanced considerably by grain refinement owing to the delay in fatigue crack initiation life under low stress amplitude [2,24]. The significance of the current study is that our experimental results on HCF performance of Cu-HEA defy the conventional expectation by exhibiting high fatigue endurance limit of ~ 700 MPa (0.62 UTS) despite its UFG condition (Fig.2b). Hence, this alloy presents an attractive combination of its tensile strength, inherent to UFG materials, as well as promising HCF

behavior. Fig.2b shows the stress amplitude (S)-number of cycles (N) curve from fully reversible (R = -1) bending fatigue testing. Fatigue tests were carried out at several stress levels, stress amplitude ranging from 637 MPa (0.57 UTS) – 840 MPa (0.75 UTS), to determine an S-N curve. The extraordinary fatigue strength of Cu-HEA is not only higher than UFG materials but also outperforms most of the fatigue-resistant materials like commercial Ti alloys and Ni-based superalloys and recently reported HEAs (Fig.2b) [6,10,12-14,25-30]. In summary, the flexibility-based alloy design of Cu-HEA displayed a fatigue runout stress amplitude (700 MPa) with a normalized fatigue ratio of 0.62 UTS. A detailed, albeit brief, investigation of fatigue failure in terms of crack initiation and propagation follows.

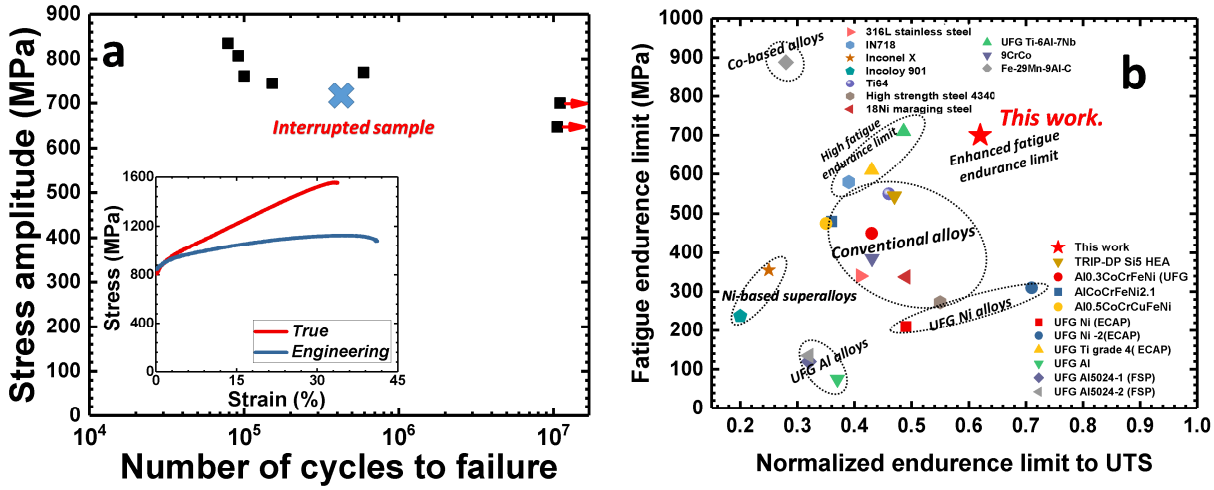

Fig. 2. Tensile and fatigue behavior. (a) S-N curve for fully reversible fatigue testing of Cu-HEA with an inset showing engineering and true stress-strain curves, and (b) comparison of the fatigue endurance limit vs. UTS for current alloy with other alloys. (UTS: ultimate tensile strength)

To understand crack initiation and its propagation path, a microstructural investigation of an interrupted specimen was carried out. A fatigue test was interrupted after 114710 cycles at 717 MPa (0.64 UTS) with an indication of an instant decrease of ~2% on one side of the stress

amplitude. As the crack starts from one surface, bending stress on that surface reduces, while that of the other surface remains constant [31]. An overall fatigue crack path is shown in Fig.3a. BSE and EBSD phase maps of different regions from the crack tip confirm transformation-induced plastic accommodation within the crack plastic zone (Figs. 3b, b_{1-3}). A lower magnification scan confirmed evidence of TRIP as observed by the significantly higher volume fraction of ε phase within the crack tip plastic zone (red region in Figs.$3b_{1-3}$). As γ→ε transformation is associated with strain mismatch between these phases, it results in alteration of localized WH behavior, which enables local enhancement of deformation accommodation at the crack tip. Important to note is that the amount of stress required to trigger the TRIP effect depends on the stability of γ phase. As a result, refined and strong γ resists ε formation until higher stress is reached [32]. Once the crack is initiated, it forms a plastic zone at the crack tip and locally alters stress distribution. Stress concentration within the crack plastic zone reaches stress levels sufficient to trigger the TRIP effect. However, stability of the γ phase is confirmed by the fact that in the absence of stress concentration, transformation is not activated outside of the plastic zone (Figs.$3b_{1-3,}$ d). This is confirmed by the almost complete γ microstructure (green) away from the crack tip plastic zone (Fig.$3b_2$) and the higher fraction of the ε phase (red) within certain distance from the crack tip (Figs. $3b_{1,3}$). Additionally, micro-crack branching (Fig. 3c) indicates increased energy dissipation by the near perpendicular propagation relative to the main crack path and therefore helps to avoid conventional abrupt fatigue failure.

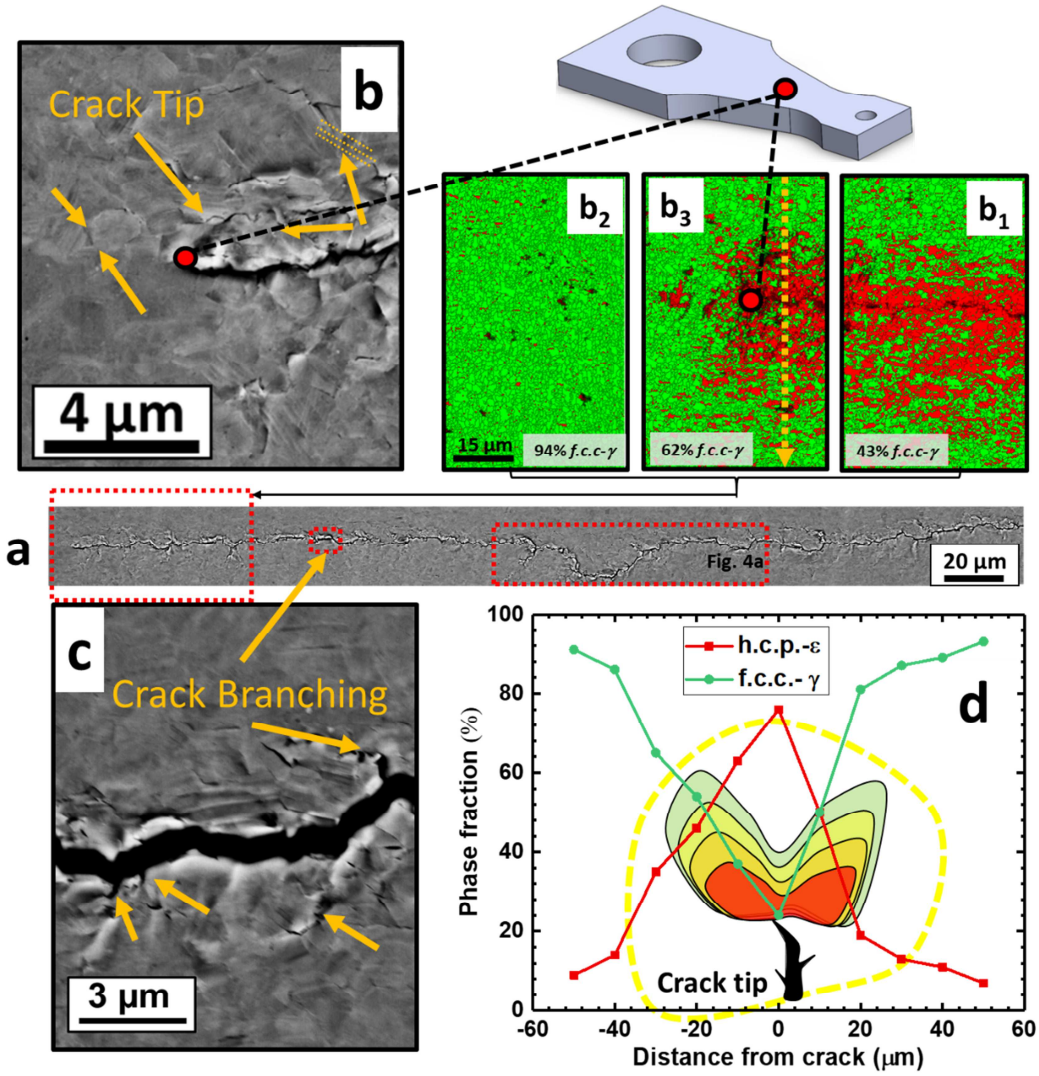

Fig. 3. Microstructural characterization for interrupted fatigue test. (a) Overview of a crack. (b) High magnification BSE image of crack tip, (b_1–b_3) EBSD phase maps reveals crack tip phase evolution due to stress concentration, (c) BSE image reveals crack branching that accounts for energy dissipation, and (d) crack tip phase evolution due to plastic zone. (BSE: backscattered scanning electron)

Typically, less fatigue-resistant materials are prone to rapid fatigue failure due to a shorter path for crack propagation. However, extensive research has been carried out to engineer the crack propagation paths by increasing the mean free path for crack movement. Conventionally this has been achieved by local WH activity to accommodate strain mismatch

between either two phases or matrix and dispersoids, thereby altering the mean free path for crack propagation. This phenomenon is termed “crack retardation.” The present work confirmed that the combination of an ultrafine grain and metastable alloy achieved similar crack retardation (Fig. 4a) owing to the localized γ→ε transformation (Figs. 4b, b_1) within the crack tip plastic zone (Fig. 4a). This transformation-induced crack retardation triggers micro-crack growth away from the main path, extends the main crack path and subsequently delays the failure. However, to sustain this localized WH activity, dynamic load transfer between the γ and ε phases results from straining even during cyclic loading [33]. Extensive cyclic plastic deformation results in additional energy dissipation during crack growth stage. The localized Kernel average misorientation (KAM) distribution suggests reasonable strain accommodation occurred within the plastic zone in the newly-formed ε phase, and confirms active involvement of the ε phase in strain accommodation with deformation twinning [34], as confirmed by the higher KAM values in the ε phase (highlighted by circles in Figs. 4c, $c_{1\text{-}2}$). Twinning dependent on chemistry as well as stress. It is claimed that twinning induced plasticity is mainly seen at later stages of plastic deformation (near UTS) due to higher level of stress required for re-orienting the γ f.c.c. matrix. Moreover, twinning also led to ε formation in metastable γ matrix because of higher stability of intrinsic stacking faults [35] . Hence, the designed alloy has relatively more metastable matrix than conventional TRIP/TWIP steels and hence showed ε formation. In short, effective plasticity within the ε phase via deformation twinning, in addition to TRIP, contributed to a more sustained localized WH activity and thus enabled deviation in the crack propagation path by formation of micro-cracks, which ultimately resists fatigue failure.

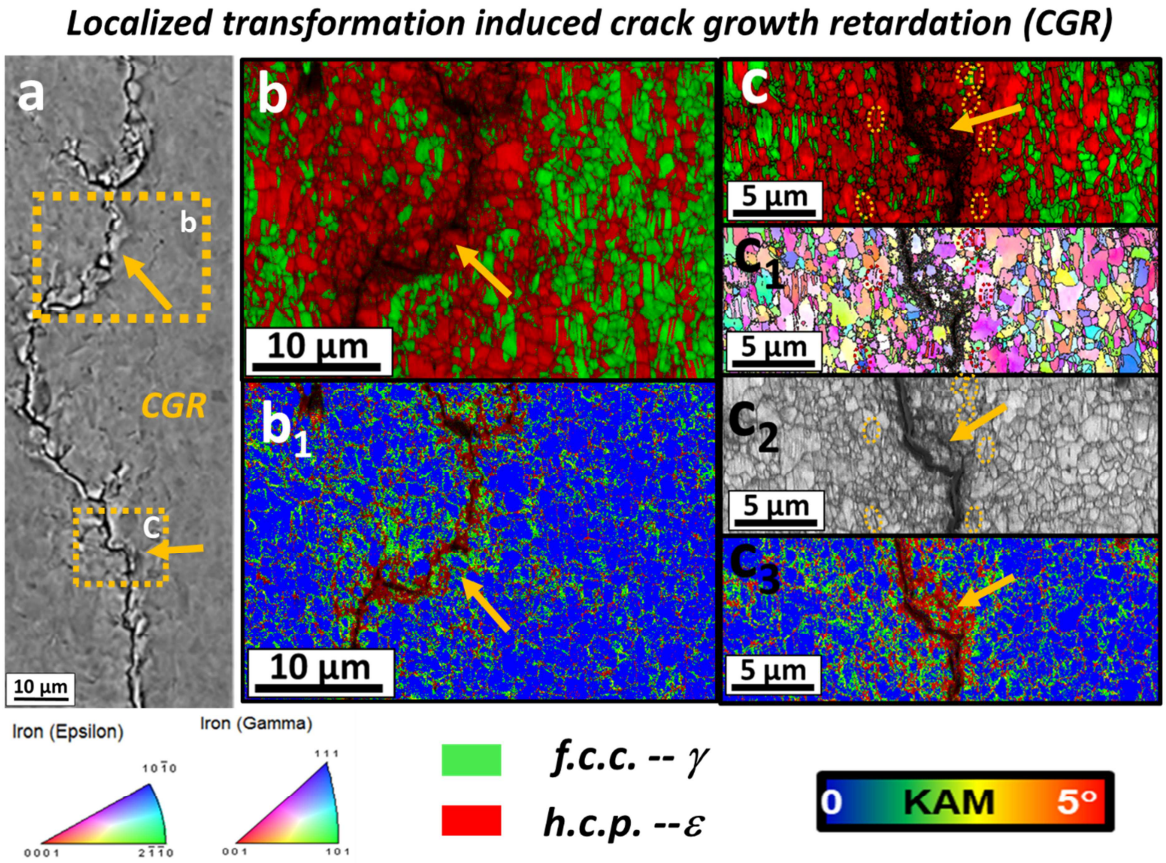

Fig. 4 Microstructural characterization reveals evidence of crack growth retardation (CGR). (a) BSE image of a crack region, (b) region b EBSD phase map shows phase distribution, (b_1) KAM analysis corresponds to (b), (c, c_1–c_3) higher magnification scan around the crack with image phase map, IPF map, image quality map, and KAM, respectively.

Conclusions

In summary, conventional materials exhibit low resistance to crack initiation and propagation rates because of limited energy dissipation during these stages. Ultrafine grained materials show delayed crack initiation but faster propagation rates along grain boundaries under high cycle fatigue regime. However, these trends were overcome in the present work by combining ultrafine grain microstructure with metastable matrix, Cu-HEA not only showed delayed crack initiation but also delayed crack propagation in the high cycle fatigue regime. This

unconventional fatigue response is attributed to the controlled TRIP effect within the crack plastic zone and effective strain accommodation by the newly-formed ε phase by slip and twinning.

Acknowledgments

Authors gratefully acknowledge the support of the National Science Foundation through grant #1435810. The authors are thankful to the Center for Advanced Research and Technology for providing access to the microscopy facilities at the University of North Texas.

Author contributions

K.L., S.S.N., M.F., S.S., R.S.M. designed the research; K.L. S.S.N., M.F. and S.S. processed and characterized the alloy; K.L., S.S.N., M.F., S.S., and R.S.M. analyzed the results; K.L., S.S.N. and R.S.M. drafted the manuscript. All authors discussed the results and contributed to the final manuscript.

Data availability statement

The raw/processed data required to reproduce these findings cannot be shared at this time as the data also forms part of an ongoing study.

References

[1] S. Suresh, Fatigue of Materials, Cambridge university press, 1998.

[2] H. Mughrabi, H.W. Höppel, Mater Res Soc Symp Proc. 634 (2000).

[3] X. Cheng, R. Petrov, L. Zhao, M. Janssen, Eng. Fract. Mech. 75 (2008) 739.

[4] P. De, C. Obermark, R. Mishra, J TEST EVAL. 36 (2008) 402.

[5] S. Nene, K. Liu, M. Frank, R. Mishra, R. Brennan, K. Cho, Z. Li, D. Raabe, Sci Rep. 7 (2017) 16167.

[6] M. Koyama, Z. Zhang, M. Wang, D. Ponge, D. Raabe, K. Tsuzaki, H. Noguchi, C.C. Tasan, Science. 355 (2017) 1055.

[7] A.P. D.Fournier, Metall Mater Trans A. 8A (1977) 1095.

[8] F. Lecroisey, A. Pineau, Metall Mater Trans B. 3 (1972) 391.

[9] G.B. Olson, M. Azrin, Metall Trans A. 9 (1978) 713.

[10] K. Liu, M. Komarasamy, B. Gwalani, S. Shukla, R.S. Mishra, Scr. Mater. 158 (2019) 116.

[11] K. Liu, S.S. Nene, M. Frank, S. Sinha, R.S. Mishra, Mater Res Lett. 6 (2018) 613.

[12] M.A. Hemphill, T. Yuan, G. Wang, J. Yeh, C. Tsai, A. Chuang, P. Liaw, Acta Mater 60 (2012) 5723.

[13] Z. Tang, T. Yuan, C. Tsai, J. Yeh, C.D. Lundin, P.K. Liaw, Acta Mater. 99 (2015) 247.

[14] S. Shukla, T. Wang, S. Cotton, R.S. Mishra, Scr. Mater. 156 (2018) 105.

[15] S. Mahajan, C. Pande, M. Imam, B. Rath, Acta Mater. 45 (1997) 2633.

[16] E.I. Galindo-Nava, P. Rivera-Díaz-del-Castillo, Acta Mater. 128 (2017) 120.

[17] S. Nene, S. Sinha, M. Frank, K. Liu, R. Mishra, B. McWilliams, K. Cho, Appl Mater Today. 13 (2018) 198.

[18] S. Nene, M. Frank, K. Liu, R. Mishra, B. McWilliams, K. Cho, Sci Rep. 8 (2018) 9920.

[19] S. Nene, M. Frank, K. Liu, S. Sinha, R. Mishra, B. McWilliams, K. Cho, Scr. Mater. 154 (2018) 163.

[20] M. Frank, S.S. Nene, K. Liu, S. Sinha, R. Mishra, manuscript under preparation.

[21] K Mageshwari, R.S. Mishra, JOM. 67 (2015) 2820.

[22] S. Nene, M. Frank, K. Liu, R. Mishra, B. McWilliams, K. Cho, Sci Rep. 8 (2018) 9920.

[23] S. Nene, K. Liu, M. Frank, R. Mishra, R. Brennan, K. Cho, Z. Li, D. Raabe, Sci Rep. 7 (2017) 16167.

[24] A. Vinogradov, Adv Eng Mater. 17 (2015) 1710.

[25] T. Niendorf, T. Wegener, Z. Li, D. Raabe, Scr. Mater. 143 (2018) 63.

[26] G.B. Olson, R. Chait, M. Azrin, R.A. Gagne, Metall Mater Trans A. 11 (1980) 1069.

[27] X. Cai, J. Feng, W. Owen, Metall Mater Trans A. 16 (1985) 1405.

[28] G. Haidemenopoulos, A. Kermanidis, C. Malliaros, H. Dickert, P. Kucharzyk, W. Bleck, Mat Sci Eng A. 573 (2013) 7.

[29] A. Wan, J. Xiong, Z. Lyu, K. Li, Y. Du, K. Chen, Z. Man, Chinese J Aeronau. 29 (2016) 1405.

[30] S. Chang, Y. Hsiau, M. Jahn, J. Mater. Sci. 24 (1989) 1117.

[31] S. Jana, R.S. Mishra, J.B. Baumann, G. Grant, Acta Mater. 58 (2010) 989.

[32] M. Wang, Z. Li, D. Raabe, Acta Mater. 147 (2018) 236.

[33] Z. Li, C.C. Tasan, K.G. Pradeep, D. Raabe, Acta Mater. 131 (2017) 323.

[34] M. Calcagnotto, D. Ponge, E. Demir, D. Raabe, Mat Sci Eng A. 527 (2010) 2738.

[35] B.C. De Cooman, Y. Estrin, S.K. Kim, Acta Mater. 142 (2018) 283.

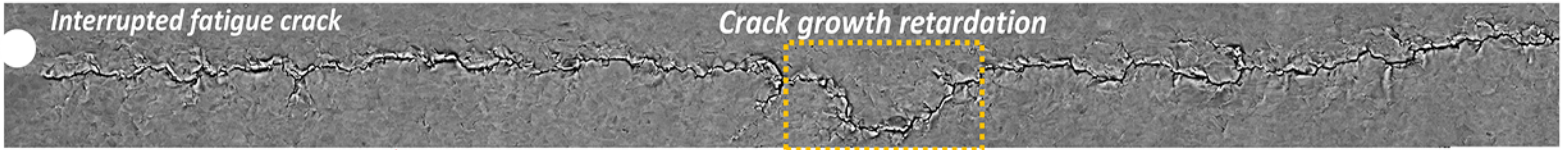
Interrupted fatigue crack
Crack growth retardation

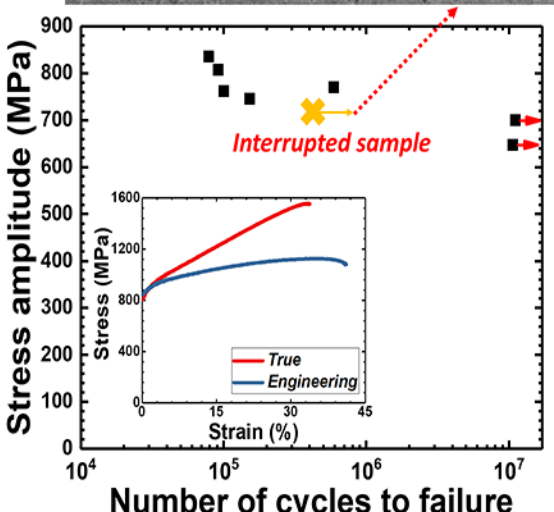
Stress amplitude (MPa)
Number of cycles to failure
Interrupted sample
Stress (MPa)
Strain (%)
True
Engineering

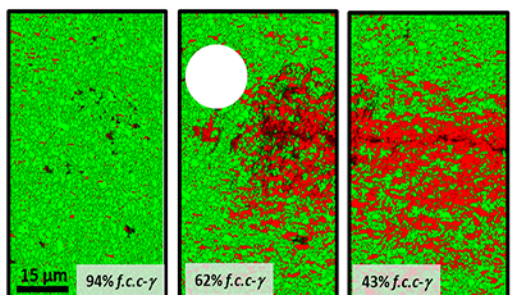
15 μm
94% f.c.c-γ
62% f.c.c-γ
43% f.c.c-γ

h.c.p. (ε) f.c.c. (γ)

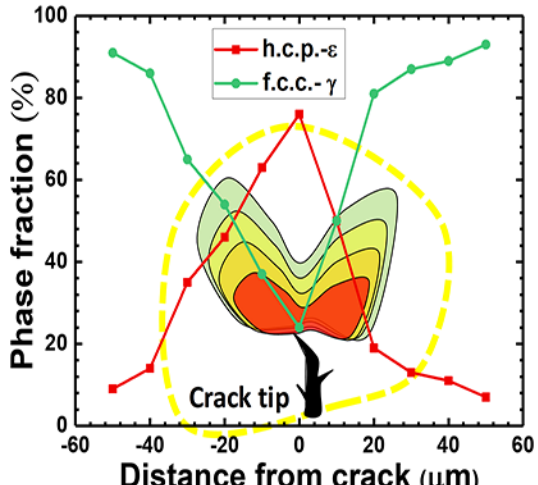
h.c.p.-ε
f.c.c.- γ
Phase fraction (%)
Crack tip
Distance from crack (μm)